

Article

An Investigation of Residual Stresses after the Turning of High-Tempered Bearing Steel

Anna Mičietová¹, Mária Čilliková¹ , Robert Čep² , Branislav Mičieta¹, Juraj Uriček¹ and Miroslav Neslušan^{1,*} 

¹ Faculty of Mechanical Engineering, University of Žilina, Univerzitná 1, 01026 Žilina, Slovakia; anna.micietova@fstroj.uniza.sk (A.M.); maria.cillikova@fstroj.uniza.sk (M.Č.); branislav.micieta@fstroj.uniza.sk (B.M.); juraj.urocek@fstroj.uniza.sk (J.U.)

² Faculty of Mechanical Engineering, VŠB—Technical University of Ostrava, 17. listopadu 2172/15, 708 00 Ostrava, Czech Republic

* Correspondence: miroslav.neslusan@fstroj.uniza.sk; Tel.: +421-908-811-973

Abstract: This study is focused on analysing residual stresses (RSs) after turning high-tempered bearing steel through the use of the X-ray diffraction (XRD) technique. Phase transformations expressed in terms of the near-surface white layer (WL) and the corresponding microhardness profiles are correlated with the RSs as well as the depth of the RS profiles. Normal and shear components of RS and *FWHM* (full width at half maximum) of the diffraction peaks are analysed as a function of cutting insert flank wear as well as the cutting speed. It was found that the influence of tool wear prevails over cutting speed, RSs tend to shift into the compressive region with increasing tool flank wear, and the valuable shear components of RSs can be found in the near-surface region when the cutting inserts of lower flank wear are employed. The increasing flank wear also increases the depth in which the compressive RSs can be found. Furthermore, surface RSs are affected by the phase transformation process (formation of re-hardened WL) as well as the superimposing mechanical and thermal load.

Keywords: turning; residual stresses; high-tempered steel



Citation: Mičietová, A.; Čilliková, M.; Čep, R.; Mičieta, B.; Uriček, J.; Neslušan, M. An Investigation of Residual Stresses after the Turning of High-Tempered Bearing Steel. *Machines* **2024**, *12*, 139. <https://doi.org/10.3390/machines12020139>

Academic Editor: Kazumasa Kawasaki

Received: 23 January 2024

Revised: 13 February 2024

Accepted: 14 February 2024

Published: 17 February 2024



Copyright: © 2024 by the authors. Licensee MDPI, Basel, Switzerland. This article is an open access article distributed under the terms and conditions of the Creative Commons Attribution (CC BY) license (<https://creativecommons.org/licenses/by/4.0/>).

1. Introduction

RSs are of vital importance with respect to the functionality of components during operation. The surfaces exposed to the cyclic load require compressive RSs not only in the near-surface layer but in the deeper layers as well since the maximum Hertz pressure can be found at a certain distance beneath the free surface [1]. The final state of RSs is very often produced during the finishing cycles, such as grinding, turning, superfinishing, etc. The development of machine tools, as well as process technology, has increased the industrial relevance of finishing turning [2], which can be used as a substitute for the grinding cycles. Hard turning can produce a very good surface state that can be expressed in terms of surface roughness [3–5] and the depth extent of microstructure transformations as well as RSs. However, progressively developed tool wear (especially the flank wear *VB* (Verhandlungs basis)) should be considered as a risk factor [6]. RSd initiated by turning cycles are due to the following:

- The non-homogenous plastic deformation of the neighbouring layers (compressive RS);
- The non-homogenous thermal expansion of the neighbouring layers (tensile RS);
- Phase transformation (compressive or tensile RS);
- A combination of the aforementioned aspects.

The turning cycles of high-tempered steels can produce a WL of variable thickness depending on the cutting conditions and, mainly, the development of flank wear *VB* [6–8]. For this reason, all of the aforementioned aspects initiating RSs should be considered. Therefore, the final RSs are driven by their superimposing contribution. The amplitude

and the direction of RSs in the different layers beneath the free surface depend on the prevailing effects listed above. Moreover, the RS state cannot be considered uniaxial, but instead, due to the remarkable differences in RSs, the cutting and feed directions should be taken into account as a result of unbalanced cutting and feed speeds. The strong imbalance with respect to process kinematics results in the preferential orientation of the matrix in the near-surface layer [6,8].

The term hard machining (hard turning) is usually associated with steels with a hardness above 50 HRC [2,6,7]. On the other hand, some aspects predominant in hard turning cycles can be found during the machining of hardened steels below this threshold as well. The formation of a surface WL (as a re-hardened matrix) [7,9] is frequently linked with the hard turning process. The WL is a product of high temperatures (exceeding the austenitising ones) followed by rapid self-cooling when VB exceeds the critical threshold [7,10,11]. RS produced by hard turning is a function of VB , cutting edge geometry, component hardness, etc. [7,12,13]. Insert flank wear VB can remarkably alter the amplitude of RSs as well as their penetration beneath the free surface [12,13].

High-tempered steel is a progressive material with an outstanding combination of mixed hardness and toughness. However, the functionality of components made of these steels especially depends on the surface state [14] expressed in terms such as RS profile, phase transformation in the near-surface layer, its phase composition, microhardness, etc. [2,12,15]. Turning operations are usually performed under constant cutting conditions. However, flank wear VB (associated with mechanical and thermal loads), as well as the corresponding stress and microstructure of the machined surface state, can vary remarkably [10,16].

This study investigates the specific character of the residual stress state with respect to the presence of shear stress. Apart from stress states, microstructure alterations in the near-surface region were also studied in terms of WL thickness or/and WL hardness. The above-listed components of surface integrity were investigated as a function of cutting speed as well as flank wear area. Their depth gradients are discussed with respect to phase transformation and non-uniform mechanical and thermal loads during hard cycles.

2. Materials and Methods

The experimental study was carried out on heat-treated bearing steel 100Cr6 with a hardness of 40 ± 1 HRC. The heat treatment of the samples was carried out under industrial conditions. Samples in the form of a disk with an external diameter of 145 mm, an internal diameter of 25 mm and a width of 25 mm were quenched in oil at a temperature of 60 °C after reaching an austenitising temperature of 840 °C and tempered for 2 h afterwards at a temperature of 530 °C. Hard face turning was carried out through the use of cutting insert DNGA 150408 made of PCBN (CBN particles, $3 \div 5$ μm ; CBN content, 70%; TiN coating) with a 0.8 mm nose radius and a chamfer angle of -35° (chamfer width: 250 μm). Inserts of variable flank wear VB (in the range from 0.05 to 0.8 mm) were prepared prior to the experiment during hard turning.

Hard turning operations are not usually performed with insert flank wear VB above 0.4 mm in order to avoid excessive cutting forces and corresponding instability in the machining. On the other hand, VB is a major factor affecting the thickness of WL as well as the penetration of RSs beneath the free surface. For this reason, quite large VB were employed. A cutting depth of $a_p = 0.25$ mm and a feed of $f = 0.09$ mm (the feed direction corresponds with the axial direction on the turned surface) were kept constant. The rotational speed of the spindle was also kept constant, resulting in a variable cutting speed through the disk diameter during face turning, as shown in Figure 1. The cutting speed v_c varied from 70 $\text{m}\cdot\text{min}^{-1}$ at a distance of approx. 8 mm from the inner diameter up to 230 $\text{m}\cdot\text{min}^{-1}$ at a distance of approx. 8 mm from the outer diameter.

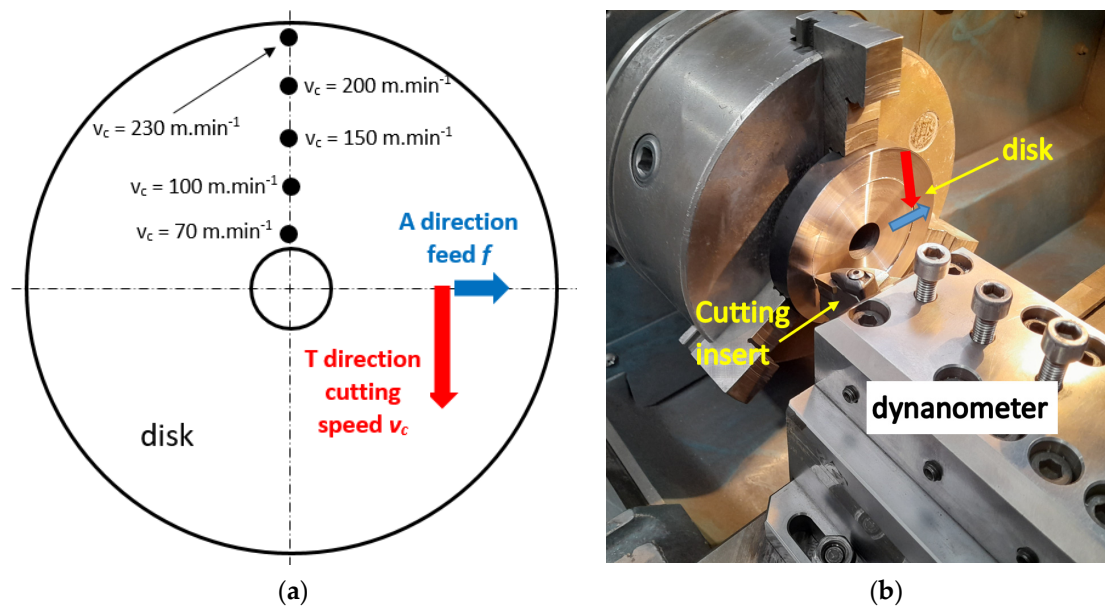


Figure 1. Brief sketch as well as the real photo of the sample with indicated directions of feed and cutting speeds. (a) brief sketch; (b) the real photo.

The RSs were measured in the tangential direction (direction of v_c , which is referred to as RS_T) as well as in the perpendicular axial direction (direction of f , which is referred to as RS_A), as shown in Figure 1. Apart from the normal component of the RSs, shear was analysed as well. The RS shear components are referred to as RSS_T in the tangential direction and RSS_A in the axial direction. The determination of RSs was performed using the XRD technique carried out on a Proto iXRD Combo diffractometer using $\text{CrK}\alpha$ radiation. The average effective penetration depth of the XRD measurements was $\sim 5 \mu\text{m}$, with a scanning angle of $\pm 39^\circ$ and a Bragg angle of 156.4° . The residual stress was calculated by examining the shifts in $\langle 211 \rangle$ reflection. The Winholtz and Cohen method and X-ray elastic constants $\frac{1}{2}S_2 = 5.75 \text{ TPa}^{-1}$, $S_1 = -1.25 \text{ TPa}^{-1}$ were used for residual stress determination. In order to analyse the stress gradients beneath the free surface, layers of the material were gradually removed via electro-chemical polishing. The thickness of the layer removed during electro-chemical polishing was measured using the MarCator 1086R digital indicator with a precision of 0.0005 mm .

To reveal the microstructural transformations induced by hard milling, 10 mm long pieces were prepared for metallographic observations (etched using 5% Nital for 8 s). The microstructure was observed in the direction of the cutting speed. Microhardness measurements of $HV0.05$ in the WL were carried out in the case of samples turned by the insert of $VB = 0.8 \text{ mm}$ since the thickness of the WL was sufficient enough for such measurements. Microhardness measurements for other samples turned by the inserts of lower VB were not carried out due to the insufficient thickness of WL. Microhardness measurements $HV0.05$ were carried out using Innova Test 400TM (50 g load; dwell time, 10 s).

Cutting force components F_c and F_p were measured through the use of the Kistler 9441 dynamometer (Kistler, Winterthur, Switzerland). The measured components were decomposed in order to extract the shear $F_{\alpha t}$ and normal components $F_{\alpha tn}$ of F_α as the net energy consumed in the VB region separated from the energy consumed for chip formation and associated with F_γ . Further details and the methodology of this decomposition can be found in the previous reports [10,17].

3. Results of Experiments and Their Discussion

Figure 2 demonstrates that VB remarkably affects the amplitude of RSs as well as their extent in terms of depth. More developed VB tends to shift the surface RS_T from the tensile region towards the compressive RS_T . On the other hand, the evolution of surface RSs is

not monotonous and straightforward due to the contribution of the non-linear evolution of cutting edge geometry with VB and the corresponding mechanical and thermal load of the surface. RS profiles for $VB = 0.6$ mm are positioned near those of $VB = 0.2$ mm since the evolution of the normal components $F_{\alpha tn}$ of F_{α} exhibits a local minimum beyond $VB = 0.4$ mm [17] (see Table 1) due to the abrupt change in the evolution of the cutting edge geometry in this region (see the previous study in which the cutting edge geometry evolution, expressed in terms of rake angle γ_n , cutting edge radius r_n , and evolution of $F_{\alpha tn}$, is reported [10,17]). It was found that the initial negative rake angle of $\gamma_n = -35^\circ$ for the new insert turns to a nearly zero geometry for the insert of $VB = 0.4$ mm, followed by a certain drop to a more negative geometry afterwards. However, this drop is compensated by the steep increase in cutting edge radius r_n , as shown in Figure 3.

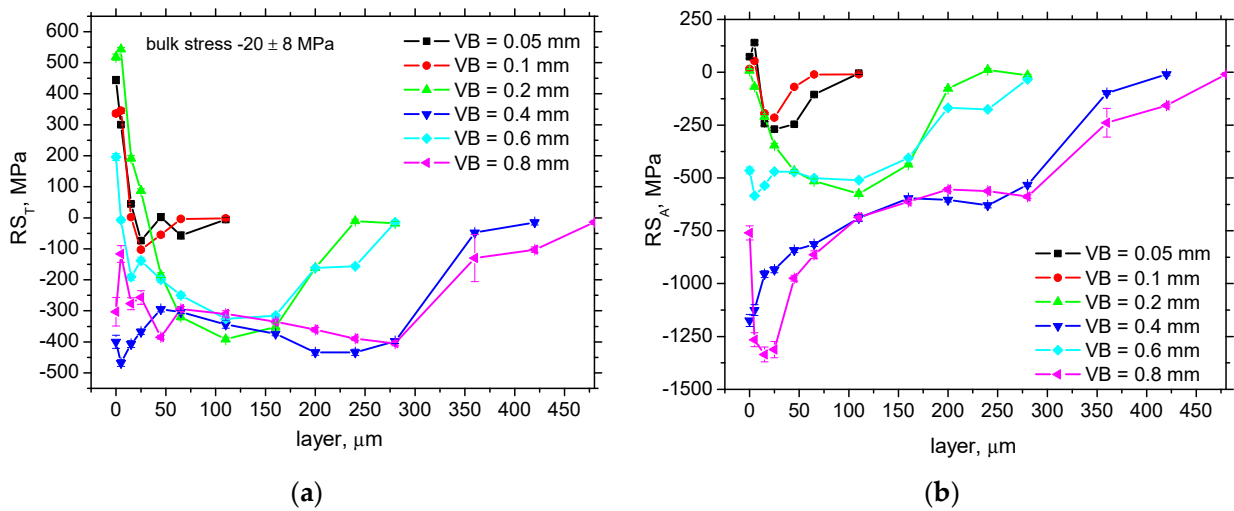


Figure 2. RS profiles as a function of VB , $v_c = 100 \text{ m}\cdot\text{min}^{-1}$. (a) RS_T ; (b) RS_A .

Table 1. Shear and normal components of F_{α} , as well as their ratio as a function of VB .

VB , mm	0.05	0.1	0.2	0.4	0.6	0.8
$F_{\alpha t}$, N	57	57	74	88	96	134
$F_{\alpha tn}$, N	164	163	282	372	365	684
$F_{\alpha tn}/F_{\alpha t}$, -	2.87	2.86	3.81	4.23	3.80	5.10

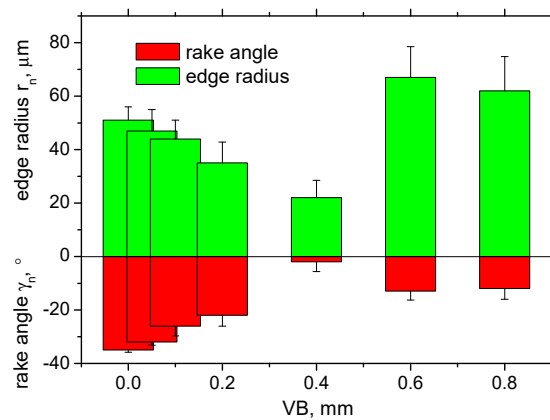


Figure 3. Rake angle γ_n and cutting edge radius r_n as a function of VB .

Progressively developed VB initiates phase transformation in the near-surface region when the matrix is heated above the austenitising temperature, followed by rapid self-cooling [18–20]. Such a thermal cycle produces a re-hardened WL, see Figure 4. The

thickness of WL increases with VB ; however, WL thickness exhibits a local minimum at $VB = 0.6$ mm (see Figure 5), and the evolution of the WL correlates with the evolution of normal and shear components of F_α and the associated alterations in cutting edge geometry, as shown in Figure 3. It should also be mentioned that the surface RS for $VB = 0.8$ mm is less compared to that of $VB = 0.4$ mm (see Figure 2a,b). The main reason can be viewed as the stress release due to the phase transformation when a certain energy associated with the non-homogeneity in the near-surface heating and stressing is consumed due to matrix dynamic recovery during rapid self-cooling. It is also worth mentioning that a WL can be found on the surfaces for all VB . However, the thickness of the WL is usually far below the sensing depth of the XRD technique apart from that of $VB = 0.4$ mm, which is quite close to the sensing depth (see Figure 5). Therefore, it is considered that the degree of surface stress relaxation grows with WL thickness.

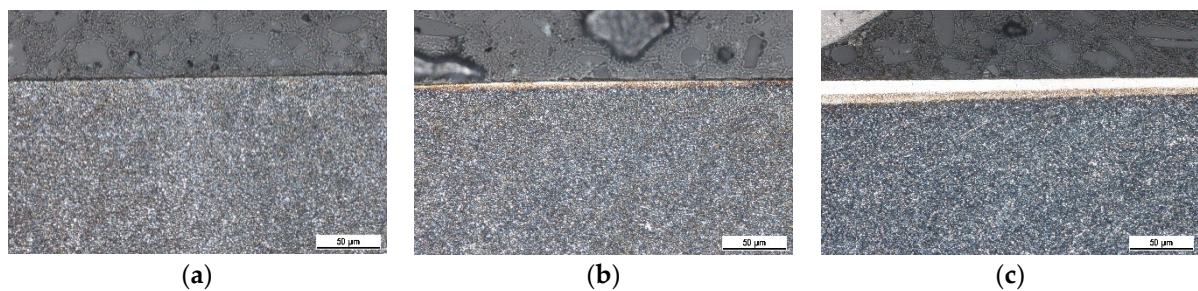


Figure 4. Some metallographic images of the machined surfaces, $v_c = 200$ m.min⁻¹. (a) $VB = 0.05$ mm; (b) $VB = 0.4$ mm; and (c) $VB = 0.8$ mm.

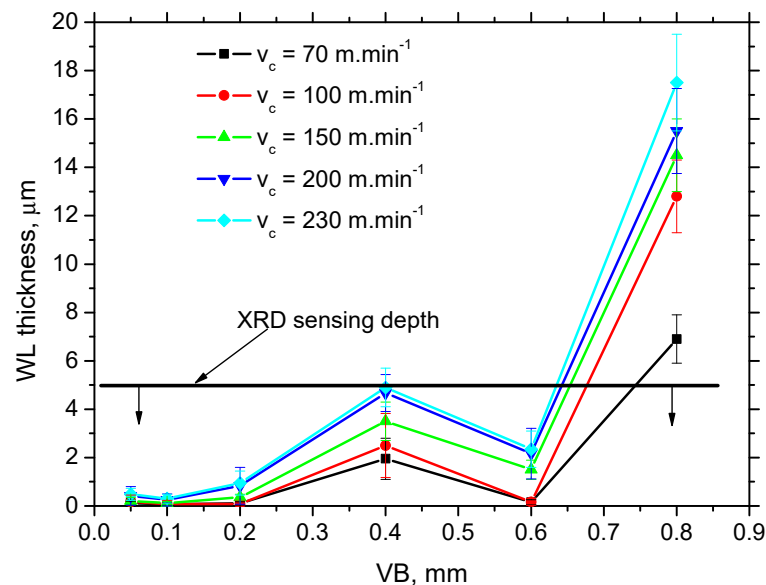


Figure 5. WL thickness as a function of VB and v_c .

Figure 2 also depicts the region in which RS is changed with respect to the bulk stress widening with VB , and the amplitude of compressive RS in the deeper layers increases with VB as well. On the other hand, the amplitude of compressive RS_A is greater compared with RS_T due to the contribution of the kinematics of the turning process (the cutting speed v_c is one order higher compared with the feed speed), preferential matrix orientation in the tangential direction [6,8] which, in turn, corresponds with the remarkable stress anisotropy [8].

Figure 6 demonstrates that the contribution of the variable cutting speed v_c is only minor, and the influence of VB remarkably prevails. Nearly the same RS profiles for the different v_c can be found for all inserts of variable VB .

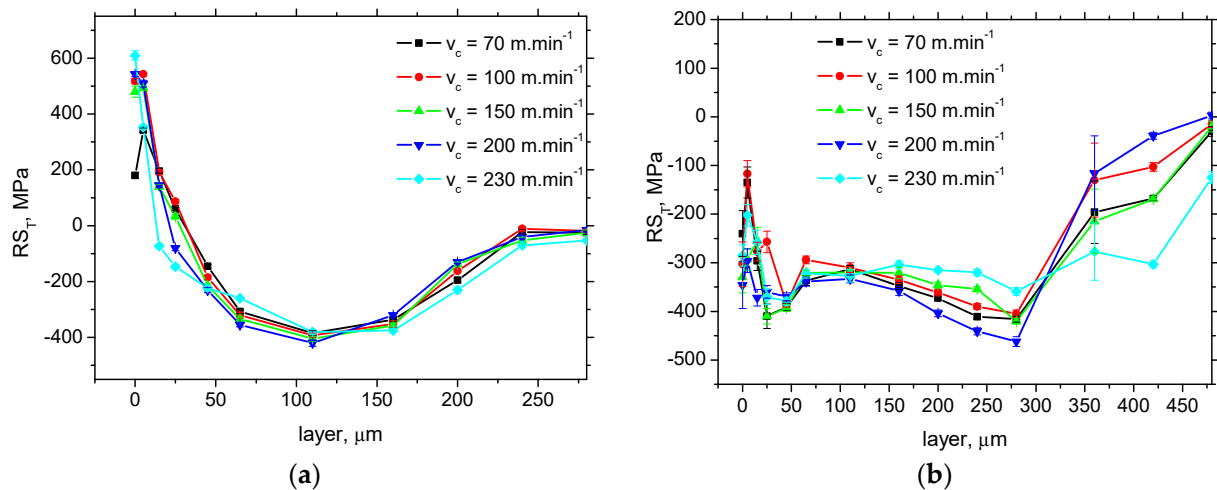


Figure 6. RS profiles in the tangential direction as a function of v_c . (a) $VB = 0.2$ mm; (b) $VB = 0.8$ mm.

Figure 7a shows that $FWHM_T$ progressively decreases with respect to the increasing depth below the free surface for all VB . It can also be noted that the $FWHM_T$ measured directly on the free surface is strongly dependent on WL thickness when the high WL thickness can be linked with the thick WL and vice versa. Moreover, the depth at which the valuable increase in $FWHM_T$ above the untouched bulk can be found increases with WL thickness. However, this parameter is mainly a function of dislocation density, and no valuable directional anisotropy for $FWHM$ measured in the direction of the cutting and feed speeds can be found.

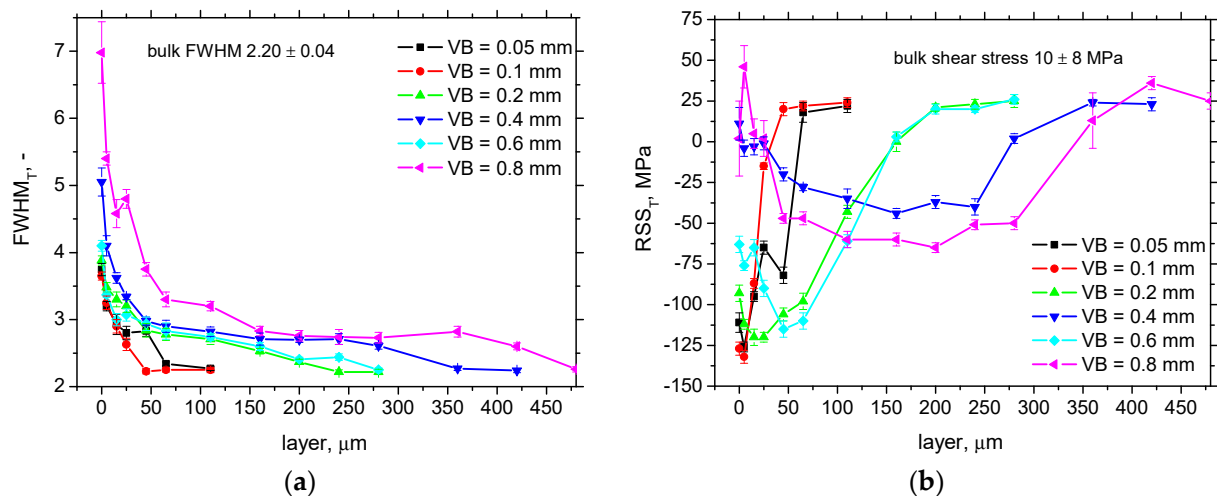


Figure 7. $FWHM_T$ of XRD diffraction peak and RSS_T as a function of VB , $v_c = 100$ m.min⁻¹. (a) $FWHM_T$; (b) RSS_T .

The evolution of RSS_T is quite interesting, as shown in Figure 7b. The surface RSS_T are indirectly proportional to WL thickness. RSS_T profiles for the thin WL (for $VB = 0.05$ and $VB = 0.1$ mm) exhibit the highest surface negative RSS_T and rapid decrease toward the bulk. RSS_T profiles for the WL of medium thickness (for $VB = 0.2$ and $VB = 0.6$ mm) exhibit medium surface negative RSS_T and a certain increase in the amplitude in the subsurface layers followed by a progressive decrease in the deeper region. Finally, RSS_T seem to be relaxed when the thickness of the WL is comparable to or higher than the XRD sensing depth, followed by a moderate increase in negative RSS_T in the deeper layers. On the other hand, RSS_A exhibit no valuable evolution, and RSS_A values more or less randomly fluctuate with respect to VB , v_c , and depth. Deeper insight into RSS s and the physical interpretation

of this parameter with respect to the turning process and the matrix produced is unclear in the current state of the art.

The XRD technique can be used in a destructive manner when depth profiles are analysed. On the other hand, XRD patterns can also be employed in a non-destructive manner when the information from the near-surface region only (which thickness corresponds to its sensing depths) is carried out. Figures 8 and 9 and Table 2 demonstrate the potential of the different XRD parameters for non-destructive monitoring of WL thickness. Figure 8a shows that the surface RS_T shifts from the tensile region towards the compressive region with increasing WL thickness (nearly the same evolution can be found for the axial direction). However, this evolution saturates when the XRD sensing depth attains the WL thickness as a result of the more developed stress relaxation in the case of a thick WL. A similar evolution expressed in terms of the correlation coefficient ρ_p can be found for RSS_T (see Figure 9a) and zero correlation for RSS_A due to the random fluctuation of this parameter with respect to VB , v_c , and depth (see Figure 9b). The best correlation can be found between $FWHM$ and WL thickness, as shown in Figure 8b.

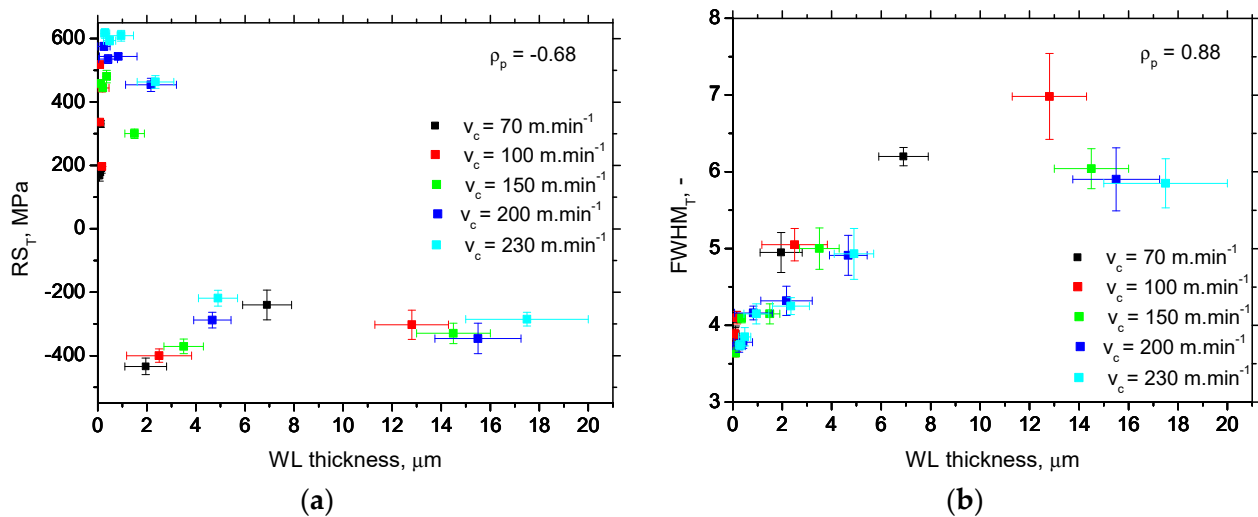


Figure 8. Surface RS_T and $FWHM_T$ versus WL thickness. (a) Surface RS_T versus WL thickness; (b) surface $FWHM_T$ versus WL thickness.

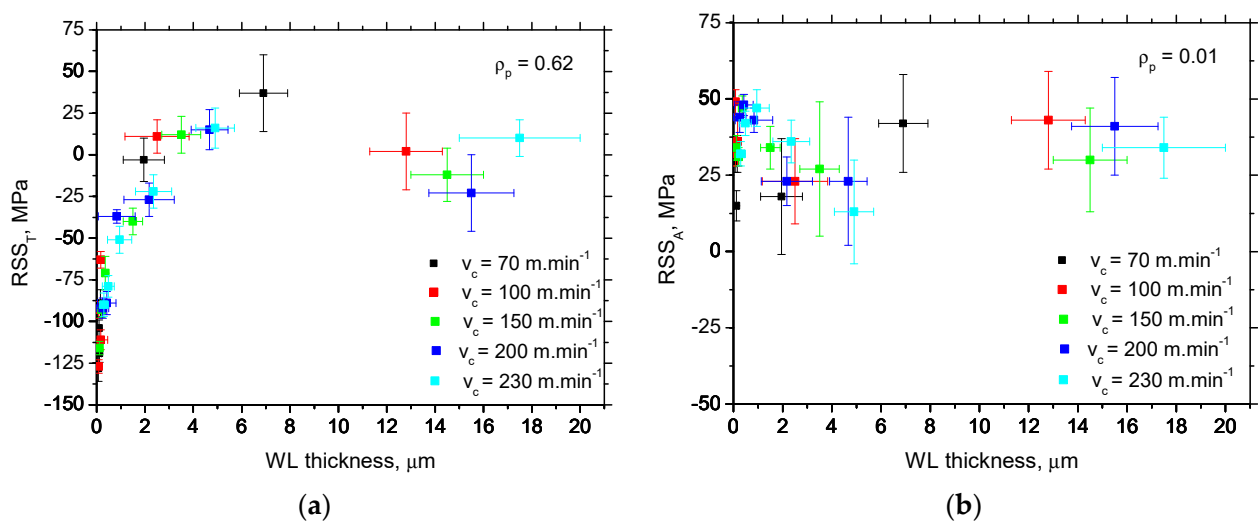


Figure 9. Surface RSS versus WL thickness. (a) RSS_T versus WL thickness; (b) RSS_A versus WL thickness.

Table 2. Correlation of the surface XRD parameters versus WL thickness expressed in terms of correlation coefficient ρ_p .

	RS	RSS	FWHM
Tangential direction	−0.68	0.62	0.88
Axial direction	−0.72	0.01	0.88

FWHM is the XRD parameter usually associated with matrix hardness, which is less dependent on the stress state and more correlated with dislocation density [21–23]. The WL thickness for $VB = 0.8$ mm is thick enough to carry out the microhardness measurements inside the WL layer, and the *HV0.05* profiles are illustrated in Figure 10. This figure demonstrates that the microhardness of the WL increases with decreasing depth due to the lower thermal load and, therefore, the higher rate of rapid self-cooling [24,25]. The influence of v_c is only minor, and the microhardness falls quite steeply toward depth. This figure also depicts that the remarkably altered RS and *FWHM* values penetrate much deeper compared to the *HV0.05* depth profiles (see also Figure 2). Therefore, correlation analysis between *FWHM* and *HV0.05* (as shown in Figure 11) should be executed at a limited depth (about 55 μm). On the other hand, Figure 7 clearly demonstrates that the steep fall of *FWHM_T* can be found just in this region. The further drop of *FWHM_T* for $VB = 0.8$ mm beyond this threshold in Figure 7 is moderate only. Figure 11 demonstrates quite good correlation between *HV0.05* and *FWHM_T* (a similar evolution can be found for the axial direction as well), and the correlation coefficient ρ_p is close to that indicated in Figure 8b. Comparing Figures 7 and 11, it can be noticed that *FWHM* exhibits a lack of sensitivity against WL thickness for $VB = 0.8$ mm with respect to variable v_c , but this parameter is sensitive to its hardness expressed in the term *HV0.05*.

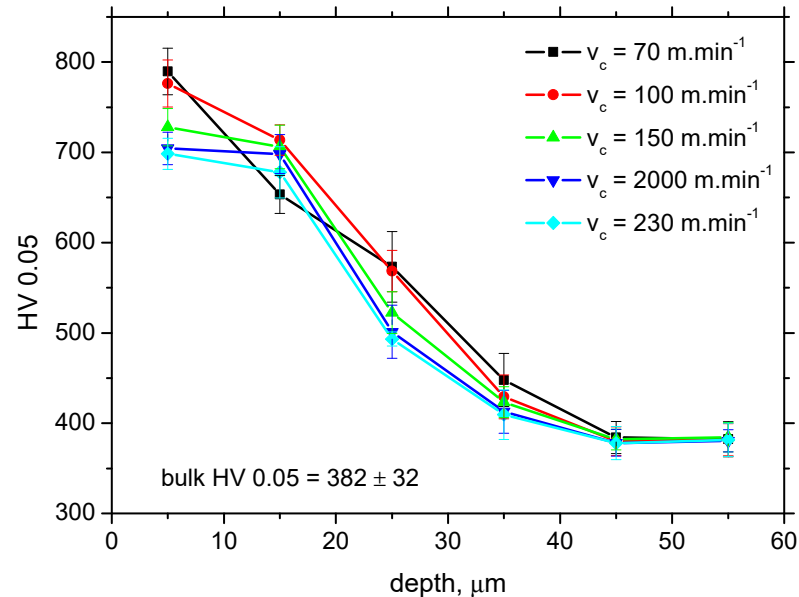
**Figure 10.** Microhardness *HV0.05* profiles for $VB = 0.8$ mm.

Figure 2 shows that the non-homogenous heating of different layers beneath the free surface prevails over the mechanical one since the surface RS_T are tensile when WL thickness is low. However, these RS_T are quite rapidly transformed into compressive ones. The contribution of phase transformation is limited due to the low WL thickness. Thermal load is driven by the specific heat Q_α' , as reported in the previous study [17]. This parameter takes into account the generated heat $Q_\alpha = F_{\alpha t}$, v_c , as well as the duration of surface heating τ (for further detail, check [14]). On the one hand, increasing VB makes the time within the surface exposed to heat longer. On the other hand, v_c increases the produced heat but

shortens τ . The shift of the surface RS_T for a thicker WL ($VB = 0.4$ and 0.8 mm) is due to the higher rate of normal component $F_{\alpha tn}$ growth along with VB compared to that of $F_{\alpha t}$ [10,17], as shown in Table 2. For this reason, non-homogenous plastic deformation dominates over thermal heating in the case of $VB = 0.4$ mm and $VB = 0.8$ mm, and the compressive surface of RS_T can be found. Although the phase transformation associated with WL formation consumes certain stress (as mentioned above), the $F_{\alpha tn}$ component still dominates over $F_{\alpha t}$, which is attributed to the thermal load via Q_α .

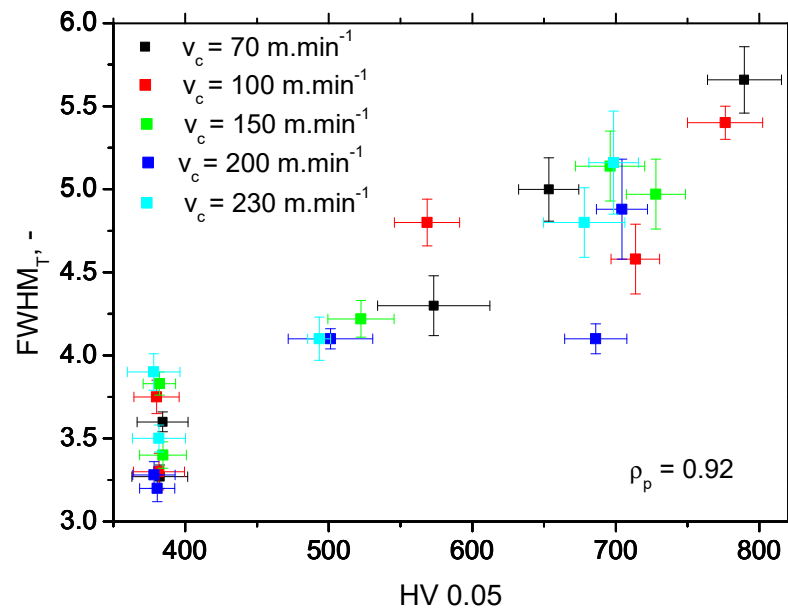


Figure 11. Microhardness $HV_{0.05}$ versus $FWHM_T$ for $VB = 0.8$ mm.

RS_T in the deeper layers are compressive, which indicates that the contribution of surface heating is vanishing and that the amplitude of the compressive RS_T , as well as their penetration depth, is driven mainly in the case of $F_{\alpha tn}$. In order to carry out the exact correlation analysis between the $F_{\alpha tn}$ and RS_T profiles, the parameters indicated in Figure 12 were proposed and analysed (taking into account the bulk stress of -20 ± 8 MPa). Figure 13, as well as the correlation coefficients of ρ_p in Table 3, indicate that the thermal effect and the associated phase transformation have a more important role in the near-surface layer. For this reason, the ρ_p for SS is lower than that of MCS. Moreover, it seems that $F_{\alpha tn}$ mainly affects DMSC as well as DB. A similar analysis of RS_A profiles as a function of $F_{\alpha t}$ and $F_{\alpha tn}$ is not possible since the shear component of F_α is not known in the axial direction. On the other hand, it is considered that this component should be remarkably lower due to the prevailing compressive RS_A .

Table 3. Correlation of parameters extracted from RS_T profiles versus $F_{\alpha tn}$ expressed in terms of correlation coefficient ρ_p (presence of the bulk stress -20 ± 8 MPa taken into account).

	SS	MCS	DB	DMCS
Correlation coefficient	-0.53	-0.72	0.90	0.93

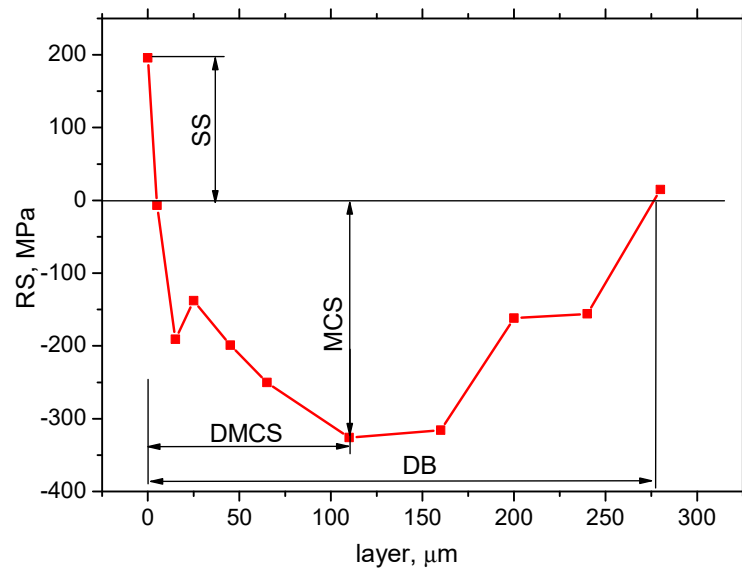


Figure 12. Parameters of the RS profile (red dots refer to the measured stress at certain distance below the free surface and red line represents the stress depth profile) correlated against F_{atn} . *SS*—surface RS; *MCS*—maximum of compressive RS; *DMCS*—distance to the maximum of compressive RS; *DB*—distance to the bulk RS.

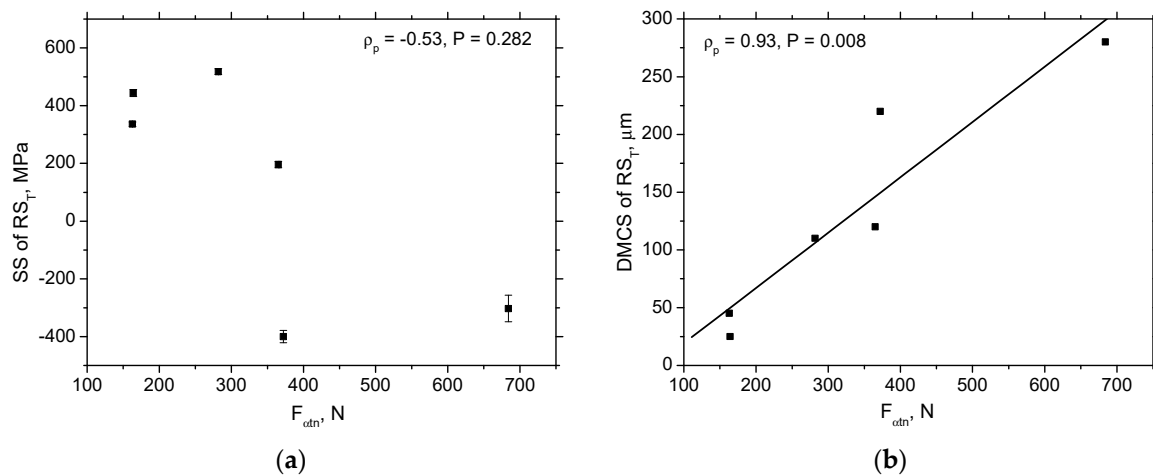


Figure 13. Correlation of parameters extracted from RS_T profiles versus F_{atn} . (a) *SS* versus F_{atn} ; (b) *DMCS* versus F_{atn} (ρ_p is the Pearson's correlation coefficient and P is the probability of obtained results).

4. Conclusions

The main findings of this study can be summarised as follows:

- Progressively developed *VB* tends to shift the surface RS_T from the tensile towards the compressive region;
- Progressively developed *VB* increases the amplitude of compressive RS_A ;
- Phase transformations associated with *WL* formation release certain stresses and contribute to the decrease in surface RS s when *WL* thickness is comparable with the XRD sensing depth;
- The *FWHM* parameter of XRD exhibits the best correlation with *WL* thickness as well as its hardness;
- Non-homogenous plastic deformation of the different layers beneath the surface prevails over the thermal effect in the deeper region mainly, and the penetration depth of compressive RS_T strongly correlates with F_{atn} .

Hard tuning cycles are very often employed early after heat treatment in order to improve the shape and geometry precision of the components. However, the final state of the surface is ground, and the combination of these competitive processes results in a reduction in time sequences during manufacturing together with an acceptable surface state. Avoiding the grinding and employment of hard turning cycles for finishing cycles might be carefully considered due to high stress and microstructure gradient in the near-surface layers. Furthermore, it should also be considered that progressively developing tool wear contributes to the surface alterations, and certain differences in surface state can be detected during the long-term usage of cutting edges. Finally, deeper penetration of the microstructure, as well as residual stress state alterations during roughing cycles, should also be avoided since the vestiges of the roughing cannot be fully removed in all cases due to the limited allowances for finishing grinding.

Author Contributions: Conceptualisation, M.Č. and A.M.; methodology, M.Č., J.U. and R.Č.; software, B.M., A.M.; validation, R.Č. and B.M.; formal analysis, R.Č., A.M. and B.M.; investigation, M.Č., M.N. and A.M.; resources, A.M. and R.Č.; data curation, J.U. and B.M.; writing—original draft preparation, M.Č., M.N. and A.M.; writing—review and editing, M.N. and A.M.; visualisation, A.M., B.M. and J.U.; supervision, M.Č. and R.Č.; project administration, M.Č. and R.Č.; funding acquisition, R.Č. and A.M. All authors have read and agreed to the published version of the manuscript.

Funding: The authors gratefully acknowledge the financial support provided by VEGA project n. 1/0052/22.

Institutional Review Board Statement: Not applicable.

Informed Consent Statement: Not applicable.

Data Availability Statement: The raw data required to reproduce these findings cannot be shared easily due to technical limitations (some files are too large). However, authors can share the data on any individual request (please contact the corresponding author by the use of its mailing address).

Conflicts of Interest: The authors declare no conflict of interest.

References

- Guo, Z.; Hao, M.; Jiang, L.; Li, D.; Chen, Y.; Dong, L. A modified Hertz model for finite spherical indentation inspired by numerical simulations. *Eur. J. Mech. A/Solids* **2020**, *83*, 104042. [[CrossRef](#)]
- Tönshoff, H.K.; Arendt, C.; Ben Mor, R. Cutting of hardened steel. *CIRP Ann.* **2000**, *49*, 547–564. [[CrossRef](#)]
- Molnar, V. Influence of Cutting Parameters and Tool Geometry on Topography of Hard Turned Surfaces. *Machines* **2023**, *11*, 665. [[CrossRef](#)]
- Gundarneeya, T.P.; Golakiya, V.D.; Ambaliya, S.D.; Patel, S.H. Experimental investigation of process parameters on surface roughness and dimensional accuracy in hard turning of EN24 steel. *Mater. Today* **2022**, *57*, 674–680. [[CrossRef](#)]
- Felho, C.; Varga, G. Theoretical Roughness Modeling of Hard Turned Surfaces Considering Tool Wear. *Machines* **2022**, *10*, 188. [[CrossRef](#)]
- Guo, Y.B.; Sahni, J. A comparative study of hard turned and cylindrical ground white layers. *Int. J. Mach. Tool Manuf.* **2004**, *44*, 135–145. [[CrossRef](#)]
- Bandt, D. Randzonenbeeinflussung beim Hartdrehen. Ph.D. Dissertation, Universität Hanover, Hanover, Germany, 1995.
- Neslušan, M.; Mičietová, A.; Hadzima, B.; Mičieta, B.; Kejzlar, P.; Čapek, J.; Uriček, J.; Pastorek, F. Barkhausen noise emission in hard-milled surfaces. *Materials* **2019**, *12*, 660. [[CrossRef](#)] [[PubMed](#)]
- Wang, J.Y.; Liu, C.R. The effect of tool flank wear on the heat transfer, thermal damage and cutting mechanics in finishing hard turning. *CIRP Ann.* **1999**, *48*, 53–58. [[CrossRef](#)]
- Neslušan, M.; Uriček, J.; Mičietová, A.; Minárik, P.; Piška, M.; Čilliková, M. Decomposition of cutting forces with respect to chip segmentation and white layer thickness when hard turning 100Cr6. *J. Manuf. Proc.* **2020**, *50*, 475–484. [[CrossRef](#)]
- Chaudhari, R.G.; Hashimoto, F. Process controls for surface integrity generated by hard milling. *Procedia CIRP* **2016**, *45*, 15–18. [[CrossRef](#)]
- Matsumoto, Y.; Hashimoto, F.; Lahoti, G. Surface integrity generated by precision hard turning. *CIRP Ann.* **1999**, *48*, 59–82. [[CrossRef](#)]
- Bedekar, V.; Voothaluru, R.; Bunn, J.; Hyde, R.S. Measurement and prediction of through-section residual stresses in the manufacturing sequence of bearing components. *CIRP Ann.* **2019**, *68*, 57–60. [[CrossRef](#)]
- Agha, S.R.; Liu, C.R. Experimental study on the performance of superfinish hard turned surfaces in rolling contact. *Wear* **2000**, *244*, 52–59. [[CrossRef](#)]

15. Hashimoto, F.; Guo, Y.B.; Waren, A.W. Surface integrity difference between hard turned and ground surfaces and its impact of fatigue life. *CIRP Ann.* **2006**, *55*, 81–84. [[CrossRef](#)]
16. Kataoka, R.; Shamoto, E. A new hypothesis of steady-state flank wear progression of cutting tools with similar geometry and its verification. *Precis. Eng.* **2023**, *81*, 183–191. [[CrossRef](#)]
17. Čilliková, M.; Mičietová, A.; Čep, R.; Jacková, M.; Neslušan, M.; Kouřil, K. Analysis of Surface State after Turning of High Tempered Bearing Steel. *Materials* **2022**, *15*, 1718. [[CrossRef](#)]
18. Hosseini, S.B.; Klement, U.; Yao, Y.; Rytberg, K. Formation mechanisms of white layers induced by hard turning of AISI 52100. *Acta Mater.* **2015**, *89*, 258–267. [[CrossRef](#)]
19. Bedekar, V.; Shivpuri, R.; Chaudhari, R.; Scott Hyde, R. Nanostructural evolution of hard turning layers in response to insert geometry, cutting parameter and material microstructure. *CIRP Ann.* **2013**, *62*, 63–66. [[CrossRef](#)]
20. Li, J.G.; Umamoto, M.; Todaka, Y.; Tsuchiya, K. Nanocrystalline structure formation in carbon steel introduced by high speed drilling. *Mater. Sci. Eng. A* **2006**, *435–436*, 383–388. [[CrossRef](#)]
21. Mittemeijer, E.J.; Scardi, P. *Diffraction Analysis of the Microstructure of Materials*, 1st ed.; Springer-Verlag: Berlin/Heidelberg, Germany, 2004.
22. Ayers, J.E. The measurement of threading dislocation densities in semiconductor crystals by X-ray diffraction. *J. Cryst. Growth* **1994**, *135*, 71–77. [[CrossRef](#)]
23. Ungár, T.; Borbély, A. The effect of dislocation contrast on x-ray line broadening: A new approach to line profile analysis. *Appl. Phys. Lett.* **1996**, *69*, 21. [[CrossRef](#)]
24. Li, D.; Dong, H.; Wu, K.; Isayev, O.; Hress, O.; Yershov, S. Effects of cooling after rolling and heat treatment on microstructures and mechanical properties of Mo–Ti microalloyed medium carbon steel. *Mater. Sci. Eng. A* **2020**, *773*, 138808. [[CrossRef](#)]
25. Anijdana, S.H.M.; Sediako, D.; Yuea, S. Optimization of flow stress in cool deformed Nb—Micro alloyed steel by combining strain induced transformation of retained austenite, cooling rate and heat treatment. *Acta Mater.* **2012**, *60*, 1221–1229. [[CrossRef](#)]

Disclaimer/Publisher’s Note: The statements, opinions and data contained in all publications are solely those of the individual author(s) and contributor(s) and not of MDPI and/or the editor(s). MDPI and/or the editor(s) disclaim responsibility for any injury to people or property resulting from any ideas, methods, instructions or products referred to in the content.